



Spectral Analysis of Event-Related Hemodynamic Responses in Functional Near Infrared Spectroscopy

CEYHUN BURAK AKGÜL AND BÜLENT SANKUR

Electrical and Electronics Engineering Department, Boğaziçi University, Bebek, Istanbul, Turkey

ATA AKIN*

Institute of Biomedical Engineering, Boğaziçi University, Bebek, Istanbul, Turkey

ataakin@boun.edu.tr

Received January 15, 2004; Revised June 29, 2004; Accepted August 24, 2004

Action Editor: Xiao-Jing Wang

Abstract. The goal of this paper is to design experiments that confirm the evidence of cognitive responses in functional near infrared spectroscopy and to establish relevant spectral subbands. Hemodynamic responses of brain during single-event trials in an odd-ball experiment are measured by functional near infrared spectroscopy method. The frequency axis is partitioned into subbands by clustering the time-frequency power spectrum profiles of the brain responses. The predominant subbands are observed to confine the 0–30 mHz, 30–60 mHz, and 60–330 mHz ranges. We identify the group of subbands that shows strong evidence of protocol-induced periodicity as well as the bands where good correlation with an assumed hemodynamic response models is found.

Keywords: near infrared spectroscopy, cerebrovascular dynamics, time-frequency distribution, oscillatory brain dynamics

1. Introduction

Functional near infrared spectroscopy (fNIRS) has been proposed as a non-invasive and rapid tool to monitor the cerebrovascular changes during cognitive tasks (for a review, see (Chance et al., 1998; Obrig et al., 2000b; Villringer and Chance, 1997). Their results have indeed confirmed that fNIRS shows explicitly the response pattern of a deoxyhemoglobin (Hb) decrease and an oxyhemoglobin (HbO₂) increase when monitored over the same area where the maximal blood oxygen level-dependent (BOLD) signal increase has been observed in functional magnetic resonance imaging (fMRI) studies. Similar to fMRI, fNIRS measures any cognitive activity indirectly via

the coupling of neuronal activation to blood flow and oxygen delivery. However in contrast, fNIRS is capable to monitor these activities on a millisecond basis at the expense of lost spatial details. The fNIRS systems use multi-wavelength illumination to extract both Hb and HbO₂ concentration changes (Boynnton et al., 1996; Obrig et al., 2000a, b).

In this paper, we aim to characterize the spectrum of fNIRS signals during a cognitive task and identify the relevant frequency bands. We define as relevant frequency bands those intervals of frequency, which are most correlated with neuronal activity associated with cognitive tasks and where protocol-induced periodicity can be observed.

Several researchers in the field of neuroimaging have investigated oscillatory behavior of hemodynamic activity. Efforts for characterizing the components in the

*To whom all correspondence should be addressed.

spectra have concentrated on establishing a physiological correspondence with the peaks or the energy bands. Functional MRI and transcranial Doppler sonography studies have proposed several association mechanisms of vasomotor dynamics while emphasizing the fact that a strong signal, the brain hemodynamic response, exists and dominates the lower portion of the spectrum computed from temporal neuroimaging data (Obrig et al., 2000a; Franceschini et al., 2000; Prince et al., 2003; Toronov et al., 2000).

In all these studies, the main goal has been to identify the spectral peaks or bands related to a given task, hence elucidate the underlying physiological dynamics and their relation to performance. This provides a means to investigate the coupling between cerebral energy metabolism and cerebrovascular dynamics (namely, neurovascular coupling). The common view is that while some of the oscillatory dynamics occur independently of any task and give rise to distinct spectral bands uncorrelated with other physiological activities (e.g. breathing, heart beat etc.), other bands are affected by psychological or pathological conditions (or vice versa) through which degradation of task performance can be monitored (Kim and Uğurbil, 2002; Franceschini et al., 2000; Obrig et al., 2000a; Toronov et al., 2000).

Several researchers used spectral estimation techniques and transfer function analysis to relate the brain hemodynamic response to various stimuli and physiological events (Villringer and Chance, 1997; Svensen et al., 2000; Wobst et al., 2001; Hu et al., 1999; Kuo et al., 1998; Giller et al., 1999). Most studies that are performed by transcranial Doppler sonography suggest low frequency domination due to cerebral autoregulation of hemodynamical activity where the increase in acidity levels (increase on carbondioxide content) leads to this very slow vasomotor activity forming the Mayer waves or the V-signal (Obrig et al., 2000a).

Functional NIRS systems collect cerebrovascular information by spectroscopic methods tuned to the main chromophores in the near infrared range (Hb and HbO₂). The simplicity of measurement system allows the fast sampling of such changes, an advantage over fMRI systems. Moreover, the ease of application of the probe and the freedom to move around are factors that alleviate the discomfort felt by the subjects during these studies. The increased level of comfort and non-invasive nature of fNIRS studies can be considered as minimization of the nuisance factors by suppressing the disrupting effects of emotions, stress and physical limitations on hemodynamic signals. Major limitation

of fNIRS systems when compared against fMRI, is the low spatial resolution. Thus in any interpretation of the fNIRS signals, the fact that these signals derive from a much wider support must be taken into consideration.

To summarize, the goals of the paper are to (i) Parse the fNIRS signal spectrum in an unsupervised and serendipitous manner based on the time-frequency spectrum, (ii) Identify the frequency bands that are most informative with respect to stimulus, and (iii) Develop a framework for choosing the set of optodes that carry relevant information on the single-event trial cognitive task. Once these fNIRS bands are identified, we believe that behavioral parameters can be better correlated with these spectral bands.

2. Preprocessing of fNIRS Signals

2.1. Data Collection

For all tasks, participants (with written informed consents) were seated in a comfortable chair in front of a computer screen in a sound-attenuated, electrically shielded room and were fitted for EEG and fNIR monitoring. Functional NIRS measurements are taken by a custom-built system developed at Dr. Britton Chance's lab at University of Pennsylvania. The system houses four LED multi-wavelength light sources and twelve photodetectors that when time and source-multiplexed constitute four non-overlapping quadruples of photodetectors (see Fig. 1). Hence in one scan of the forehead a total of sixteen measurements at each wavelength can be acquired totaling to 48 optic signals. The source and detectors are equidistantly placed on the probe as seen in Fig. 1. The probe is positioned such that the base of it aligns with the eyebrows of the subject and the middle with the Fz location from EEG electrode placement and a sports bandage is used to secure it on its place and eliminate background light leakage. Taking into consideration Firbank and et al.'s study (Firbank et al., 1998), a pre-determined source detector separation of 2.5 cm was used to account for an average adult cortex depth around 1.5 cm that allowed us to probe the first couple of millimeters of the gray matter (Firbank et al., 1998; Boas et al., 2001). Notice, however, that only one fNIRS sequence results from the processing of the recordings at three wavelengths.

It was argued that a modified version of the Beer-Lambert law could be used to determine the concentrations of hemoglobin agents from raw fNIRS measurements (Villringer and Chance, 1997). We

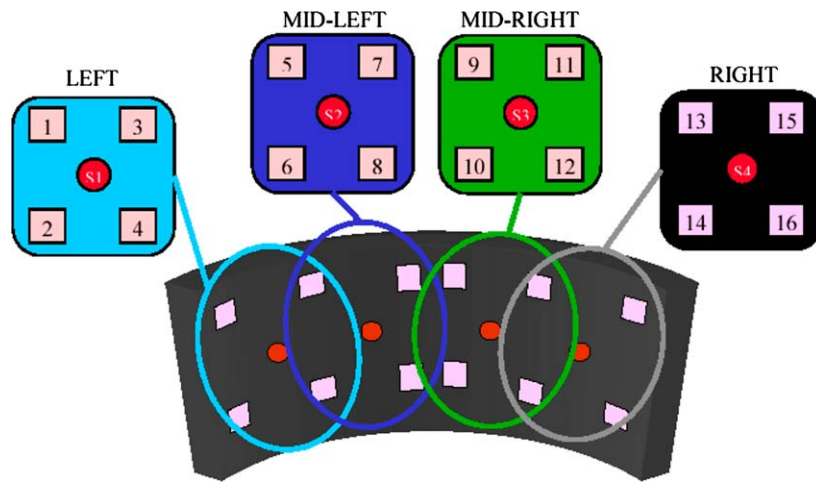


Figure 1. Source-detector configuration on the brain probe and nomenclature of photodetectors.

considered the oxyhemoglobin (HbO_2) agent, based on a recent study, where it was demonstrated that a strong correlation exists between blood-oxygenation-level-dependent fMRI data and diffuse optical HbO_2 data (Strangman et al., 2002). Thus, our measurement data consist of the time series of the HbO_2 signal samples.

Target categorization or “oddball task” is a simple discrimination task in which subjects are presented with two classes of stimuli in a Bernoulli sequence in the center of the screen. The probability of one stimulus is less than the other (e.g. 20% of trials for the “target” or “oddball” stimulus, versus 80% of trials for the “typical” or “context” stimulus); the participants have to press a button when they see the less frequent of the two events. Stimulus categories are varied, beginning with the letters “XXXXX” versus the letters “OOOOO”. 1024 stimuli are presented 1500 ms apart (total time, 25 minutes); a target is presented on 64 trials, with a minimum of 12 context stimuli in between to allow for the hemodynamic response to settle. Therefore the rest of the stimuli (960) are context cases. Subjects are asked to press the left button on a mouse when they see “OOOOO” and right button when they see the target “XXXXX” (McCarthy et al., 1997). This timing parameter is used as the behavioral reaction parameter tracking the performance of the subjects. Five male subjects with an age range of 22–50 are recruited for the preliminary test. Protocol is approved by IRB of Drexel University and MCP Hahnemann University (now Drexel University College of Medicine). We have the following additional specifications for target stimuli:

- (i) In a given experiment, overall 64 target stimuli are presented. The stimuli follow a block periodic temporal pattern, where in every block there are 8 stimuli with randomly jittered locations. However, the same pattern is repeated in every one of the eight blocks during the course of the 25-minute experiment. In other words, the inter-arrival patterns between the 1st and 8th target stimuli repeat themselves successively between the 9th to 16th, 17th to 24th and so on up to 57th and 64th.
- (ii) Inter-target interval is a random variable uniformly distributed on the (30 to 50) sample interval, or alternately on the (18 to 29) second interval.

Duration of stimuli of both context and target types is 500 ms, hence there are blank intervals of 1 second. Prior to digitization, analog optical density signals are filtered by an RC filter with 330 mHz cut-off frequency. Hence although recording is done at a sampling rate of 1.7 Hz, (the Nyquist bandwidth is 850 mHz), we consider that the 3-dB bandwidth is 330 mHz.

We had five human subjects for which the target categorization experiments were carried out. We observed that some of the detector outputs were not usable, due to either severe motion artifacts or occasional defects of the sensor. Our rejection criteria were based on visual investigation: one sort of defect was clipping in the signal amplitudes due to saturation of sensors; another was the outliers due to head movements of subjects. We also observed that, in some cases, sensors did not give any measurement at all due to hair occlusions. After eliminating the improper measurements, we ended

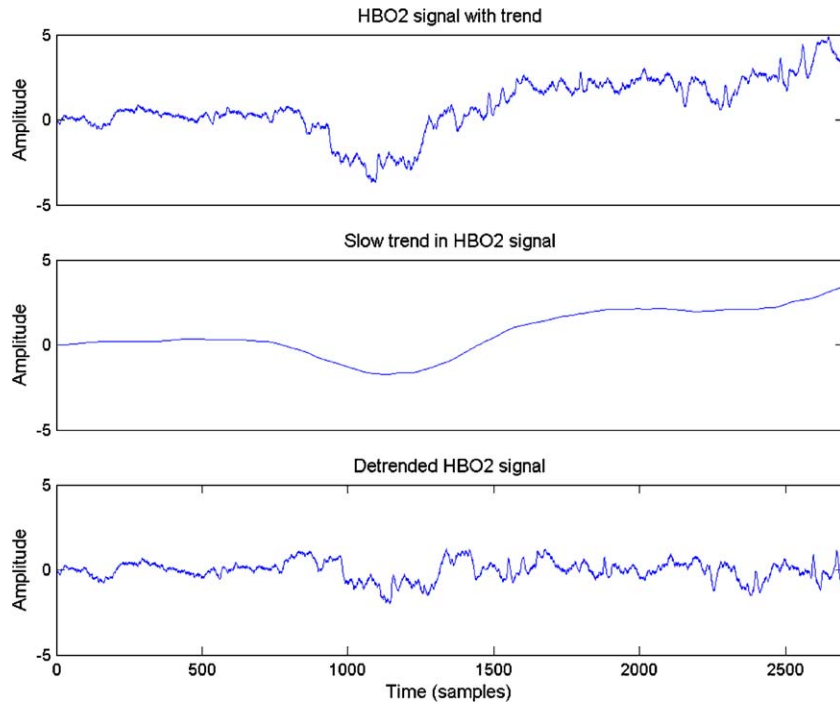


Figure 2. The effect of detrending on a typical HbO₂ signal.

up in a collection of 72 fNIRS-HbO₂ time series out of the planned $5 \times 16 = 80$ recordings. These signals were detrended, which effectively removed the very low frequency components below 3 mHz. Simple moving average filtering and subtraction of the local average perform the trend removal: a frame of support 500 samples (corresponding to 4.9 minutes of data) is slid continuously over the time-series and the mean value of the samples inside the frame is subtracted from the actual value at the frame position. The effect of such a detrending scheme is illustrated in Fig. 2. In summary, for signal characterization of the fNIRS signals we have used the 72 detrended series, each consisting of approximately 2700 samples, corresponding to duration of the cognitive task experiment of about 25 minutes.

2.2. Signal Characterization

In this section, we discuss features that characterize the fNIRS signals $\{s(t)\}$. Specifically, we search for informative bands and then explore periodicities in these bands corresponding to the target quasi-periodicity.

We conjecture that the fNIRS time-frequency spectrum can be partitioned into characteristic subbands.

The feature that we use in characterizing these subbands is the relative power time series for each band. Similar time profiles of subband energies were used in the analysis of epileptic seizure-induced EEG series (Blanco et al., 1995).

We start by estimating the time-frequency representation (TFR) in terms of the short-time Fourier transform (STFT), defined as

$$S(\tau, f) = \int_{-\infty}^{\infty} s(t)w_D(t - \tau)e^{-j2\pi ft} dt \quad (1)$$

where $s(t)$ denotes the fNIRS signal of interest and $w_D(t)$ is a window of finite support D . The short-time Fourier transform (STFT) in (1) is actually computed using the *discrete Fourier transform* (DFT), so that the TFR is discrete in both time and frequency, respectively, with time resolution Δt and frequency sampling interval Δf . A short-time transform is warranted since the signals are nonstationary and also because we want to capture and characterize local events, like brain hemodynamic response in the course of the fNIRS process. The windowing $w_D(t)$ guarantees the local nature of the spectral analysis and its support is chosen so that within that D interval the process can be considered

Table 1. Parameters of TFR, sampling rate $F_s = 1700$ mHz.

Parameter	Value	Comment
Window type	Rectangular	Rectangular window has the best frequency resolution
Window length D	60 samples ≈ 35 s	This window size provides for 28.3 mHz frequency resolution
Time resolution Δt	5 samples ≈ 3 s	The analysis is slid by steps of 5 samples, an adequate time resolution.
Frequency sampling Δf	1 mHz	Thus each 30 mHz subband has 30 representative samples.

to be at least wide-sense stationary. Table 1 gives the parameters used in the TFR analysis.

We remark that the frequency resolution is given by the effective window length, hence it is of the order of $F_s/D \approx 28$ mHz, while the 1 mHz frequency sampling rate Δf is obtained by interpolation, that is padding the windowed time series with zeroes.

We consider the evolutionary power spectral density within the n th frequency band at the instant t as

$$B_n(t, f) = S^*(t, f)S(t, f) \quad \text{in } f \in (f_{n,l}, f_{n,h}) \quad (2)$$

where $f_{n,l}$ and $f_{n,h}$ denote, respectively, the lower and upper limits of the band and the superscript $*$ stands for complex conjugation. In our case we took $f_{n,h} - f_{n,l} = 30; \forall n$. Thus this initial partitioning of the frequency spectrum has 11 bands of width 30 mHz, which collectively cover the 330 mHz bandwidth. The 30 mHz initial width of the bands is dictated by the achievable resolution after windowing the time-series data. The window size of 60 samples provides frequency resolution of 28 mHz.

The total power in a band as a function of time can be calculated by

$$I_n(t) = \int_{f_{n,l}}^{f_{n,h}} B_n(t, f) df \quad (3)$$

Similarly the total instantaneous power in the whole signal bandwidth $I(t)$ is defined as

$$I(t) = \int_{f_l}^{f_h} B(t, f) df \quad (4)$$

where, in our case, the integration goes from 3 to 330 mHz. The lower limit is dictated by detrending, while the upper limit by the cut-off frequency of the RC filter which operates prior to digitization. Finally,

the relative power profile in the n th band as a function of time becomes:

$$R_n(t) = \frac{I_n(t)}{I(t)} \quad (5)$$

The relative power profile per band reflects the temporal evolution of the relative power in each band. Two bands are considered to be distinct if the evolutions of their relative power profiles are dissimilar. Conversely, two bands are merged into one if their $R_n(t)$ responses are close to each other. Dissimilar bands that have different time evolution of the profiles, $R_n(t)$ are considered to provide different information.

3. Selection of Relevant Frequency Bands by Clustering

3.1. Band Selection Methodology

We adopt an agglomerative approach, by starting with a fine partitioning of the frequency spectrum, and then grouping bands similar in their evolutionary power profiles, $R_n(t)$, into wider bands that hopefully capture significant signal information. To express the relative power time-series from different bands and detectors/subjects, let's adopt the following notation:

$R_n^m(t)$: time-series of *relative power profile time-series* for the n th band of the m th fNIRS signal.

Thus the subscript n denotes the frequency band of interest, where $n = 1, \dots, 11$, which covers the frequency range $[(n-1) \times 30, n \times 30]$ mHz. The superscript m points to one of the $m = 1, \dots, M (M = 72)$ time-series in the database. Recall that these time series were obtained from the 16 detectors of the 5 subjects, after some pruning. We will refer to the superscript m as simply the m th measurement. The time index t runs with the lags of $\Delta t = 5$ samples, $t = 1, \dots, T$. It will be convenient to express the whole time-series $R_n^m(t)$, $t = 1, \dots, T$ in vector notation as \mathbf{R}_n^m . Thus the T -dimensional \mathbf{R}_n^m vector denotes the time series of the m th detector/subject in the n frequency band. Notice that we have a total of $N \times M = 11 \times 72$ such \mathbf{R}_n^m vectors, each detector being expanded onto 11 bands, and conversely, there are 72 representative time-series for each band.

We search for the formation of the bands by a clustering procedure. In fact, we use a scheme based on agglomerative clustering and majority voting as described below. We apply clustering to the N bands of each measurement m so that the set of N subbands

$\mathbf{R}^m = \{\mathbf{R}_n^m\}_{n=1,\dots,N}$ are clustered into C subbands $\mathbf{Q}^m = \{\mathbf{Q}_c^m\}_{c=1,\dots,C}$. Specifically the 11 initially chosen subbands from any detector/subject are clustered into $C = 3$ subbands. We have decided for this target number of three clusters to allow for a possibly very low frequency band, a high frequency band and potentially a single “interesting” mid-band.

The agglomerative clustering on data set \mathbf{R}^m has the following steps:

- (i) Initialize: Assign each vector \mathbf{R}_n^m to its own cluster.
- (ii) Compute all pairwise distances between clusters.
- (iii) Merge the two clusters that are closest to each other.
- (iv) Return to step (ii) until there are only three clusters left.

There are two important aspects in such a clustering algorithm: the *metric* used to compute distances and the *closeness criterion* between vectors. In this study we adopted the *One-Minus-the-Normalized correlation coefficient* as the distance metric

$$d(\mathbf{R}_p^m, \mathbf{R}_q^m) = 1 - \frac{\langle \mathbf{R}_p^m, \mathbf{R}_q^m \rangle}{\|\mathbf{R}_p^m\| \cdot \|\mathbf{R}_q^m\|} \quad (6)$$

where $\langle \cdot, \cdot \rangle$ stands for the inner product of two vectors and $\|\cdot\|$ for the Euclidean norm. The vectors involved in the computation are made zero-mean by subtracting their mean value. Furthermore, we adopt the *single linkage criterion* as the closeness criterion. Accordingly, the pair of adjacent bands (p, q) for which $d(\mathbf{R}_p^m, \mathbf{R}_q^m)$ is minimum are merged.

The end product of clustering the \mathbf{R}^m set is a dendrogram \mathbf{D}^m , a hierarchical tree that helps us to visualize cluster relationships. An example is shown in Fig. 3. The dendrogram for the m th measurement \mathbf{D}^m is pruned in order to get the clustered set \mathbf{Q}^m . This is accomplished by simply obtaining the cutset of the dendrogram that yields the target number of C clusters. In other words, the dendrogram is cut, as shown in Fig. 3 at a distance value, that is the ordinate, to yield the desired number of clusters. Within each one of the C clusters, the merged bands are similar to each other according to the chosen correlation coefficient metric, while across clusters they are dissimilar. The leaves of the dendrogram, that is the singleton clusters, which correspond to the initial bands, become thus grouped into $C = 3$ larger bands.

Once the agglomerative clustering is accomplished we obtain M dendrograms, one for each measurement. To extract a single set of subbands from the M clusterings we resort to a voting scheme. At this stage there

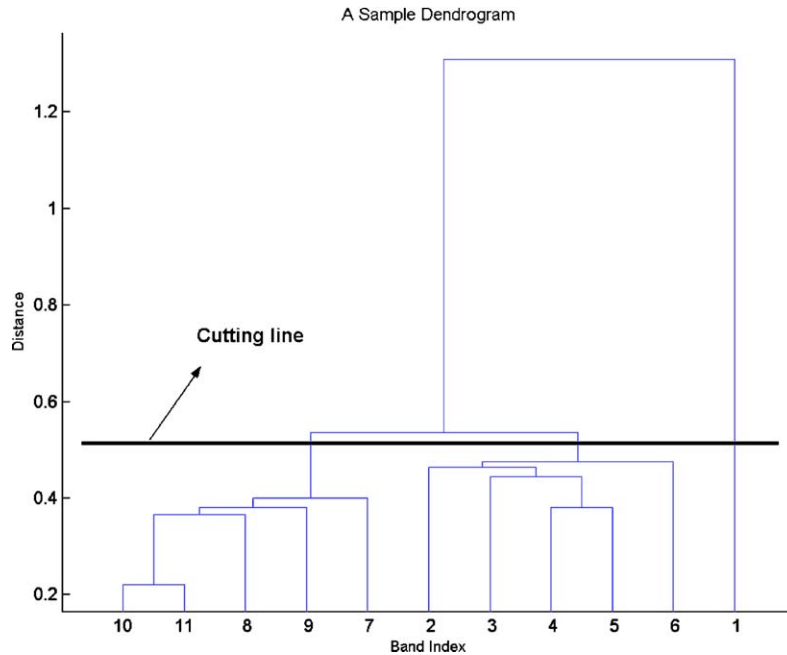


Figure 3. A typical dendrogram: The horizontal axis indexes the initial bands, vertical axis indicates with pairwise cluster distances.

are $C \times M = 3 \times 72 = 216$ candidate bands with possibly differing bandwidths, out of which we try to determine the most frequently occurring ones. We therefore rank these band patterns based on their frequency of occurrence. To make this point clear, let's consider again the sample dendrogram in Fig. 3, which results in the following subbands: $\{0\text{--}30 \text{ mHz}, 30\text{--}180 \text{ mHz}, 180\text{--}330 \text{ mHz}\}$. We determine how many times each of these subband formations are generated by the clustering of all the \mathbf{R}^m measurements, each occurrence counting as a vote. Selecting the subband patterns that have received the highest number of votes (frequency of occurrence), we achieve a partitioning of fNIRS frequency spectrum, where the resulting bands are non-overlapping and exhaustively cover the frequency interval 0–330 mHz.

3.2. Results of Band Grouping

As a result of clustering and voting, we obtained 9 candidate bands that shared 216 votes, as shown in Table 2.

Based on the results of Table 2, there are many alternative ways to partition the spectrum. Nevertheless, there is one obvious choice that exhibits the strongest evidence with 186 votes (86.1% of the total): this partition is 0–30 mHz, 30–60 mHz, 60–330 mHz. We believe that this partitioning is characteristic of fNIRS power profiles. Hereafter we call them as “canonical frequency bands” and denote them by letters A , B , C as in Table 3. Similarly when we say that we used the AB -band, BC band or ABC band, or that the signal was prefiltered in the AB -band etc we mean the band stretching, respectively, in the 0–60, 30–330, 0–330 ranges.

Table 2. Candidate bands (total number of occurrences is 216).

Band	(mHz)	Votes	Percentage (%)
0	30	72	33
30	60	57	26
30	90	11	5
30	180	3	1
30	120	1	0
60	330	57	26
90	330	11	5
120	330	1	0
180	330	3	1

Table 3. Canonical fNIRS spectrum bands.

Bands (mHz)	0–30 A	30–60 B	60–330 C
Votes	33%	26%	26%

4. Characteristics of the Canonical Band Signals

Once the canonical bands are determined, we set ourselves three goals:

- (i) To compare the cross-correlations of the relative power profiles in different bands and to discuss the physiological meaning of these bands.
- (ii) To explore the existence of any periodicity in the temporal patterns within the bands. This is relevant because the stimuli are quasi-periodic and in some of the bands, we expect that periodicity subsists more heavily than in the others. The intent of this periodicity search is to corroborate the evidence that the fNIRS does indeed measure cognitive activity, as will be demonstrated in Sections 4.2 and 4.3.
- (iii) Finally, to correlate and to fit fNIRS waveform excerpts collected right after target onsets and the Gamma function, a model for brain hemodynamic response function popular in fMRI studies.

4.1. Interpretation of the Canonical Bands

In several other studies, three main frequency bands of interest have been identified for cerebral hemodynamics: a very low frequency VLF (8–33 mHz), a low frequency LF (around 100 mHz) named as the Mayer waves or V-signal (Mayhew et al., 1999; Obrig et al., 2000a), and a high frequency component HF (around 250 mHz), the latter being definitely synchronous with breathing rate (Kuo et al., 1998). Similarly, we conjecture that each of the canonical bands is associated with one or more of the physiological activities related to hemoglobin concentrations. The lowest frequency A band (0–0.03 Hz) is mainly responsible for the slow baseline signal that is thought to be reflecting the very slow vasomotor activity due to heart rate fluctuations and thermoregulation (Toronov et al., 2000; Francheschini et al., 2000; Giller et al., 1999). In fact, reports on the frequency content of such fluctuations have identified this signal as being the phasic dilation and contractions of “the small regulating arteries, and these vasomotor waves produce fluctuations in cerebral

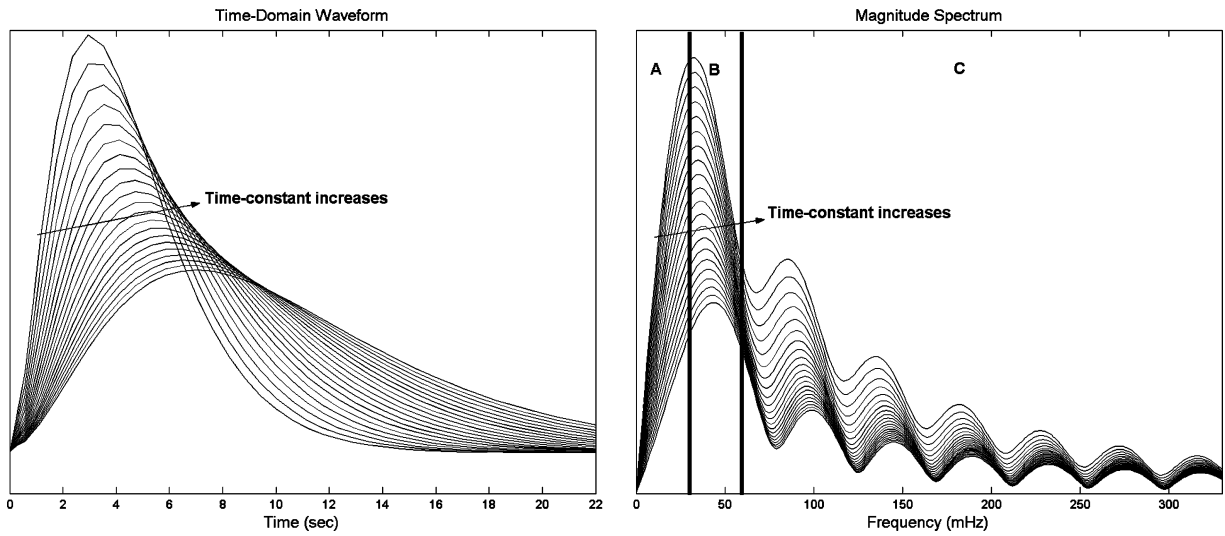


Figure 4. A family of Gamma waveforms with various time-constants (left) and their magnitude spectra (right). (The spectral sidelobes are an artifact due to centering operation).

blood volume, which are eventually reflected in the intracranial pressure” (Kuo et al., 1998). Similarly, in many fMRI studies, the Gamma function model has been used to parameterize the brain hemodynamic response. In Fig. 4, we display a family of Gamma waveforms (see Eq. (13)) with different time-constants, their magnitude spectra, on which we have superimposed the limits of the *B*-band. Since the brain hemodynamic model response, e.g. the “centered” Gamma function, has its peak located within the 30–50 mHz range (see Fig. 4), the narrow *B*-band should be related to task-related cognitive activity of the subject (Cordes et al., 2001; Toronov et al., 2000). The larger *C*-band is also assumed to carry cognitive activity related information, most probably due to the periodicity of the target stimuli sequence as we will explore more in detail in the next section. Moreover, vasomotion and breathing rate are two other physiological factors that are responsible for the emergence of the *C*-band. The *C*-band in our findings is compatible with the components of cerebral autoregulation identified by others (Cordes et al., 2001; Zhang et al., 1998; Strik et al., 2002; Giller et al., 1999).

When we consider the three bands found by our algorithm and the spectra of the BHR model as in Fig. 4, we observe that most of the energy of the Gamma waveform resides in the *B* band, followed, in order, by the bands *A* and *C*. It is of interest to consider the cross-correlations between the *R*-series within the bands. To this end, we consider the relative power time series

$R_n^m(t)$, $t = 1, \dots, T$, where m ranges over the M measurements, but n now ranges over the 3 canonical bands *A*, *B*, *C*; hence for band *A* we will use the notation $R_A^m(t)$ and similarly for the others. Cross-correlations between these series are given in matrix form below:

$$\begin{bmatrix} & A & B & C \\ A & 1 & -0.65 & -0.79 \\ B & -0.65 & 1 & 0.21 \\ C & -0.79 & 0.21 & 1 \end{bmatrix}$$

We can observe that there exists a negative correlation (correlation coefficient of minus 0.79) between the *A*-band and *C*-band. This implies that an increase in power in one band (say *A*) causes depletion of power in the other band (*C*), and vice versa. In this sense the time series $R_A^m(t)$ and $R_C^m(t)$ are almost “antipodal”. A representative triad of *R*-series in these bands is shown in Fig. 5, where the antipodality can be observed when curves in the *A* and *C* bands are superposed. The correlation coefficients between these time-series suggest a negative feedback control between the cerebral autoregulatory activities (*C*-band) and the slow frequency components (*A*-band). One conjectures that the *A*-band signals are generated partly by the cognitive activity and partly by oscillations of the cerebral spinal fluid (CSF), which has been associated with intracranial pressure oscillations in the 8–40 mHz band and are dubbed as the *B*-waves (Strik et al., 2002).

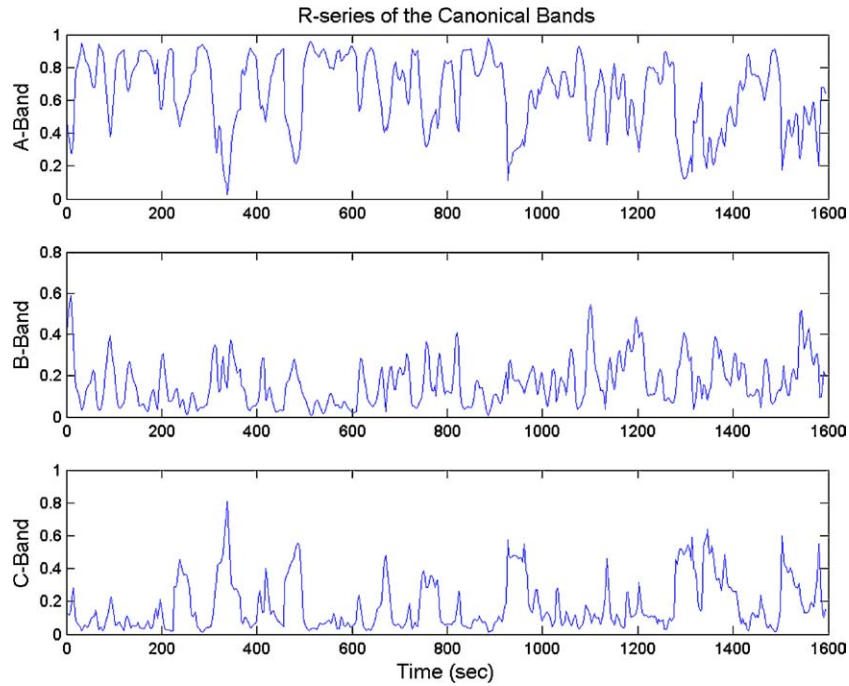


Figure 5. A representative set of R -series in the canonical bands.

Due to the probe geometry and physics of photon migration in tissues, it is most likely that the detectors are picking up a weighted sum of all the hemodynamic activities lying underneath each detector, namely the skin dynamics, cranium and CSF dynamics, and lastly, the cortex dynamics.

4.2. Search for Periodicities

Since the cognitive stimuli are quasi-periodic, whose target presentation intervals are uniformly distributed between 18–29 seconds, we can expect some sort of periodic behavior in the cognitive activity signals. The frequency bands in which such periodic response emerges more distinctly can be thought to better reflect cognitive activity or the “brain hemodynamic response.” Recall that the brain displays continuous activity (baseline activity) patterns even in the absence of any cognitive task. The cognitive activity waveforms, if any, will be in general immersed in the baseline activity. In fact, cognitive activity responses are very difficult to discern by simple observation of the waveforms. It follows that classical Fourier spectrum, correlation and peak picking techniques are not suitable for hunting these responses and more sophisticated statistical

methods must be invoked to detect and estimate these hidden periodicities (Toronov et al., 2000).

We analyze the bands $\{A, B, C\}$ and search for periodicities. The admissible periods should be in the vicinity of target exposition periods of the experimental protocol, that is, in the 18–29 seconds range or its harmonic/subharmonic multiples. Recall that, any periodicity in the time domain will emerge as discreteness (line spectrum) in the frequency domain. Thus, if a time-domain signal is periodic with P_0 (18 to 29) seconds, the corresponding spectrum should exhibit spectral samples $1/P_0$ Hz (34 to 59 mHz) apart. Since the B -band can at most accommodate one such spectral line, we merge the two bands B and C , to cover the 30–330 mHz band range. Previous researchers (Kuo et al., 1998; Giller et al., 1999; Hu et al., 1999) have also excluded the A -band since it was mostly mirroring the fNIRS baseline activity. Another plausible argument for excluding the A -band is that it is inherently a nonstationary process, which obviates signal-processing tools requiring stationarity. To this effect, we used a zero-phase finite impulse response (FIR) high-pass filter with unit gain and a 3 dB transition bandwidth of 1 mHz at 30 mHz. We will denote the corresponding band-pass filtered signals for simplicity as $x(t) = s_{BC}(t)$.

The periodicity measure we adopted is based on a classical method to estimate the pitch period in speech signals: the least-square periodicity estimation (LSPE) (Friedman, 1977). It is simply based on the minimization of the weighted mean-squared error (MSE) between the observed signal $x(t)$ and an estimated signal $x_0(t)$ that satisfies $x_0(t) = x_0(t + kP_0)$, $t = 1, 2, \dots, T$ and $k = 0, 1, \dots, K = \lfloor T/P_0 \rfloor - 1$ where $\lfloor \cdot \rfloor$ denotes the floor operation. The optimal $x_0(t)$, for a given P_0 , is

$$x_0(t) = \frac{\sum_k x(t + kP_0)w(t + kP_0)}{\sum_k w(t + kP_0)} \quad (7)$$

where $w(t)$ is the weight sequence of length T . Observe that (7) reduces to the following if all signal samples are equally weighted, i.e. $w(t)$ is a rectangular window,

$$x_0(t) = \frac{1}{K} \sum_k x(t + kP_0) \quad (8)$$

It has been argued that the weight sequence should be selected so that it has the maximum value of unity at the center of its support and that it decays smoothly down to zero towards the extremes since the period deviates more heavily at the extremes than at the center. It has been shown that P_0 that minimizes the weighted MSE is, equivalently, the one that maximizes the functional:

$$J_1(P_0) = \frac{I_0 - I_1}{E - I_1} \quad (9)$$

where I_0 stands for the weighted energy of the estimate $x_0(t)$ and E for the weighted energy of the original signal $x(t)$, and where $I_1(P_0) = \sum_t \frac{x^2(t)w^2(t)}{\sum_k w(t+kP_0)}$. Note that the LSPE with J_1 -index is also called as the pseudo-maximum likelihood estimation of periodicities (Friedman, 1977).

In (9), we search for the dominant period in the signal, \hat{P}_0 , that maximizes the $J_1(P_0)$ functional provided the periodicity index $J_1(P_0)$ is adequately high. In fact, the index function can be interpreted as a confidence score that becomes 1 only for a truly periodic signal. Since some maximizing value of \hat{P}_0 can always be found, for this estimate to correspond to a genuine periodicity, the confidence score should exceed a minimum threshold. Based on the protocol parameters we allow \hat{P}_0 to take values between P_{\min} and P_{\max} . Since the cognitive stimuli are not exactly periodic and since, furthermore, the cognitive activity signals are heavily embedded in baseline signals, we do not expect $J_1(\hat{P}_0)$

scores to be high, and hence we avoid heavy thresholding. A final confounding factor to be taken into account is that the cognitive response may not be fired exactly after the target presentation, but some variable delay may occur.

In order to illustrate the viability of the LSPE algorithm, we use a simulated data sequence that consists of the superposition of a Gamma waveform train embedded in white noise (the signal-to-noise ratio is 10 dB) and of an actual signal copied from the *A*-band. The average period of Gamma waveforms is 40 samples with a uniform random jitter between $(-10, 10)$ samples in order to simulate our experimental protocol (see Fig. 6).

Figure 7 illustrates the advantage of filtering out the *A*-band signal and to run the periodicity detector only in the *BC* band. It can be seen that the index values become higher when the band *A* is removed from the signal.

The results of the periodicity estimation on real data are presented in Fig. 8. In this particular case without prefiltering (*ABC* bands), the periodicity could not even be detected with any reasonable confidence, while in the filtered case (*BC* bands) we observe that a periodicity is detected in the expected range with acceptable confidence (Fig. 8).

In order to prospect the actual fNIRS-HbO₂ data for periodicities, we run the LSPE algorithm session by session, since the experimental protocol consists of eight identical sessions in succession. That is, we consider each of the eight sessions of the experiment separately and apply Eqs. (7)–(9). We use for each session a superscript $j = 1, \dots, 8$, so that $\{x^j(t)\}$ denotes the j th experimental session in the 30–330 mHz band-pass filtered fNIRS signal from whatever subject/detector. The session-wise processing of the fNIRS signal, together with prefiltering within the *BC*-band, helps also to mitigate the nonstationarity of these signals. In fact, we may view the signal portions in different sessions as independent realizations of the target categorization experiment if we neglect any correlation due to the baseline signal, which is independent of the cognitive activity. The hunting for periodicity maxima proceeds as follows:

- (i) The range in which we search for periodicities is $(20, 60)$ samples.
- (ii) We look for local maxima of the $J_1(\hat{P}_0)$ functional; furthermore, once a peak is found, no further peak is searched within its neighborhood of $(-3, 3)$ samples.

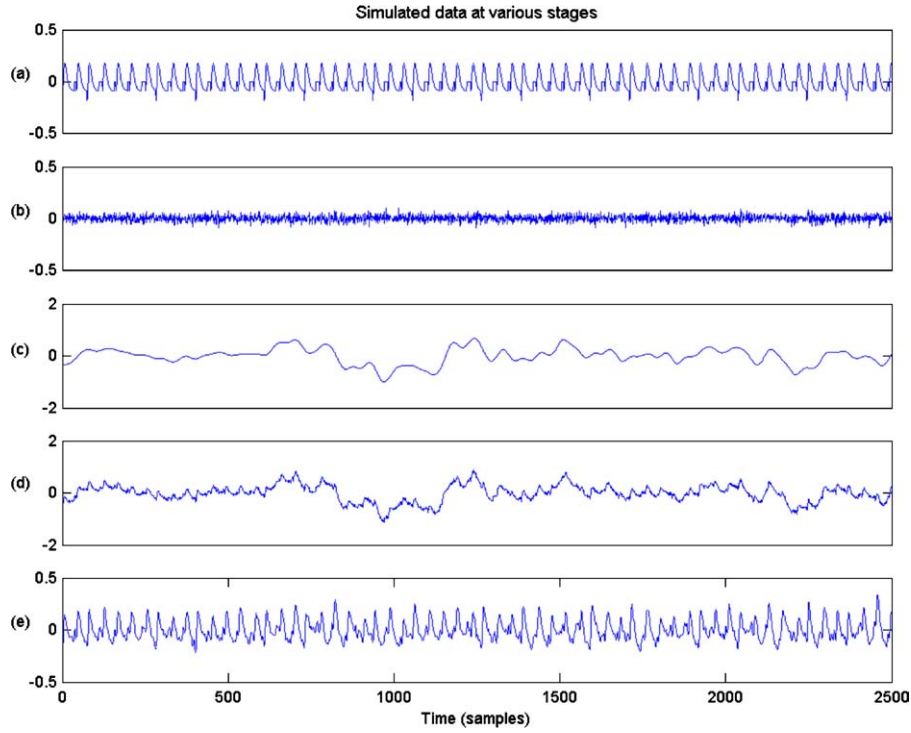


Figure 6. (a) Simulated quasi-periodic sequence of cognitive activity waveform; (b) white noise sequence (SNR = 10 dB); (c) an actual A-band signal; (d) superposition of the signals in (a), (b) and (c); (e) Band-pass filtered version of (d) in the BC-band: this signal is then used for periodicity detection.

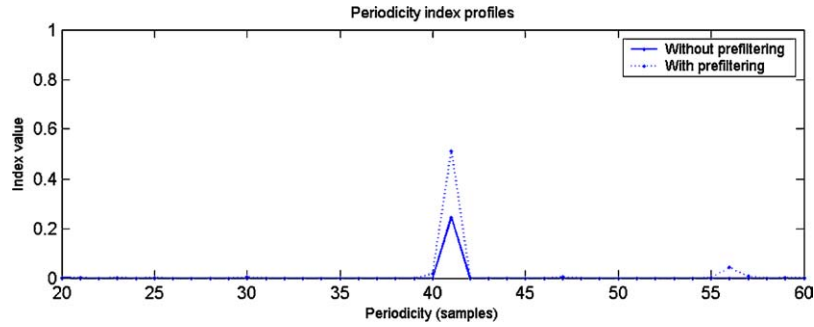


Figure 7. Periodicity index profiles for simulated data without prefiltering (solid line) and with prefiltering (dotted line), after local maxima selection and thresholding.

- (iii) We set a threshold of 0.1 on the periodicity belief value $J_1(\hat{P}_0)$.
- (iv) For each signal portion, we let the algorithm return the periodicity estimate with largest J_1 -index.

Those \hat{P}_0 values that fall within the (30, 50) samples interval are thought to belong to the single-trial cognitive activity in the experiment. Those falling outside are considered as fortuitous values, indicative of the fact

that that detector is not capturing properly any cognitive activity signal during that session. Since there are 8 session signals $x^j(t)$ per detector (each in turn possessing 8 target stimuli), each $\{x(t)\}$ signal returns eight period estimates, \hat{P}_0^j , $j = 1, \dots, 8$ along with their confidence scores. We accumulate separately the scores of the periodicities falling, respectively, inside and outside the expected range. We define the cumulative score of inside periodicities S_{in} and the count of

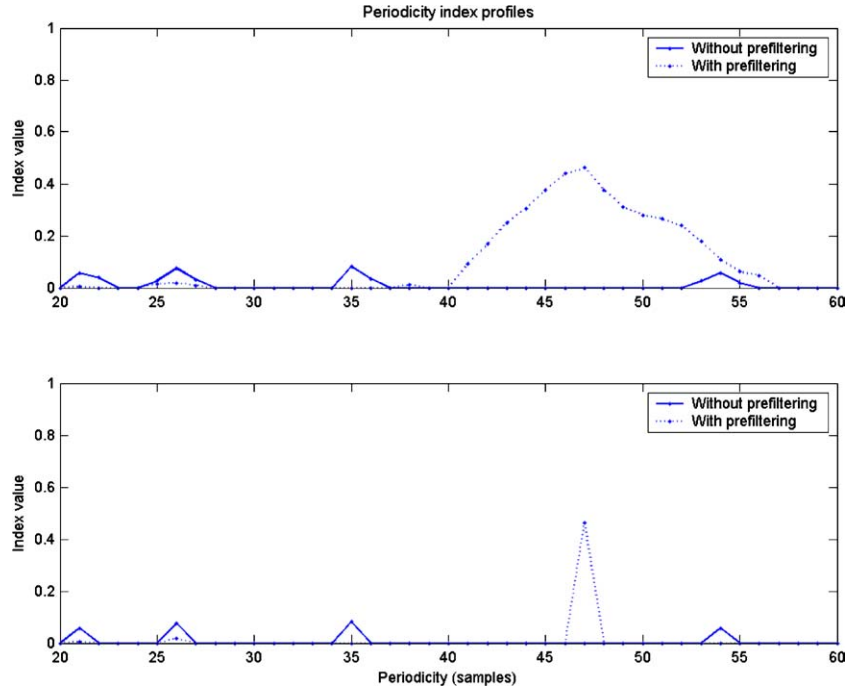


Figure 8. Periodicity index profiles with (dotted line) and without (solid line) prefiltering (top), after local maxima selection and thresholding (bottom): thanks to prefiltering out band A, a periodicity with a good confidence emerges within the expected range.

inside periodicities C_{in} for a given detector and target categorization experiment as:

$$S_{in} = \sum_{j=1}^8 J_1(\hat{P}_0^j) \delta(\hat{P}_0^j) \quad (10)$$

$$C_{in} = \sum_{j=1}^8 \delta(\hat{P}_0^j) \quad (11)$$

with

$$\delta(\hat{P}_0^j) = \begin{cases} 1 & \text{if } \hat{P}_0^j \text{ is inside the expected range} \\ 0 & \text{if } \hat{P}_0^j \text{ is outside the expected range} \end{cases} \quad (12)$$

where $j = 1, \dots, 8$ is the session index. Similarly we define corresponding expressions for the outside periodicities S_{out} and C_{out} . Furthermore, in order to investigate intersubject and interdetector variability of periodicities, we compute two quantities: periodicities falling in the proper range averaged over all subjects for a given photodetector, denoted as $\bar{P}_{subject}(k)$, $k = 1, \dots, 16$, and inside periodicity averaged over all photodetectors for a given subject, denoted as $\bar{P}_{detector}(l)$, $l = 1, \dots, 5$. The error bar plots corresponding to these two quantities, $\bar{P}_{subject}(k)$, $k = 1, \dots, 16$ and $\bar{P}_{detector}(l)$, $l =$

$1, \dots, 5$, are displayed in Fig. 9. We also show the bar plots of the scores and the scatter plots of the detected periodicities with respect to the photodetector number in Fig. 9.

Several conclusions can be drawn from these results:

- (i) The averaged period estimates match the expected value of P_0 , whether the average is computed over detectors or subjects, as illustrated in Fig. 9.
- (ii) For any detector or subject there is some dispersion of estimated periodicity values. The large spread, of the order of 10% in each sense, may be due to the jitter of target instances, to the presence of context activity, and to the limited observation interval containing, at most, eight target stimuli.
- (iii) We have also a method to classify detectors as responsive of BHR periodicity and the non-responsive ones, that is, those detectors that do not show any evidence of periodicity within the expected range. The discrimination method is based on the not-in-the-range periodicity score, as illustrated in Fig. 10, over subjects 1 to 5. The reason why some detectors do not yield conjectured periodicity could be due to the lateralization effect for

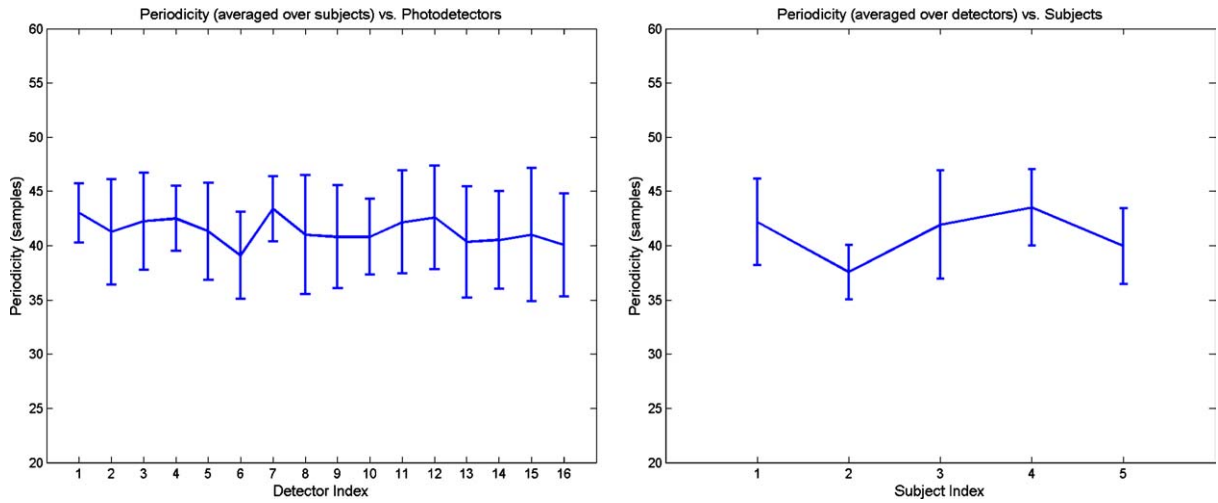


Figure 9. Plots of \bar{P}_{subject} (left) and $\bar{P}_{\text{detector}}$ (right), the bars indicate the inter-quartile range of data, computed over admissible (that is, within-range) cases.

that subject or simply to corrupted measurements. One argument that supports lateralization conjecture is that adjacent detectors all succeed or fail in a group. For example, for Subject 1, detectors 3–12 are “good”, while detectors 1–2 and 13–16 are “bad” (see Table 4). One other reason could be due to the location of the optodes with respect to the light sources. Since the source-detector distribution determines the volume of brain being sampled, millimeter range shifts and alignments in the probe will result in a significant change in the brain volume being monitored. Finally, the corruption observed could be due to the skin effects (larger arteries on the skin surface right underneath the optode) dominating the signal.

- (iv) There are also marked differences between subjects. For example, Subjects 1, 3 and 4 (especially Subject 4) yield high periodicity scores con-

sistent across all their detectors, while Subjects 2 and 5 are dubious. Although inter-subject variability is always expected in such studies, there is no standard procedure to isolate corrupted data from statistical analysis for fNIRS signals. The periodicity analysis method provided in this paper might be used as a rule of thumb in identifying the corrupted data or the patient that is not cooperating.

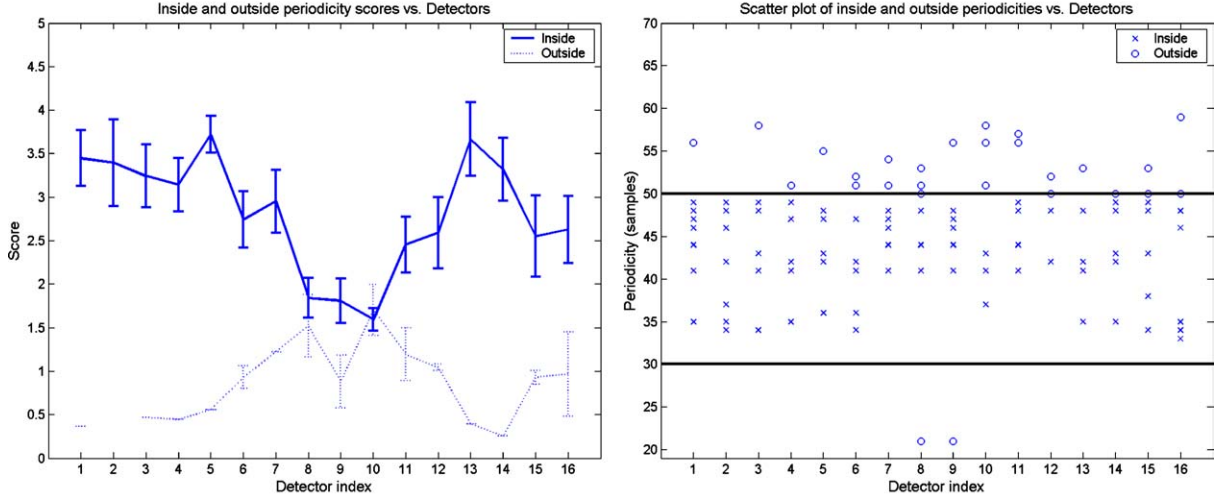
4.3. Correlation Analysis

We have seen in Section 4.2 that fNIRS possesses evidence of cognitive activity as reflected in the periodic patterns of target stimuli. We can further explore such activity by correlating with our data a brain hemodynamic response model, as borrowed from fMRI

Table 4. Photodetectors with S_{in} higher than S_{out} .

Subject	Photodetector quadruples			
	Left (1–4)	Mid-left (5–8)	Mid-right (9–12)	Right (13–16)
1	3 and 4	5 to 8 (all)	10, 11 and 12	16
2	-not any-	8	9, 11 and 12	13 to 16 (all)
3	4	5 to 8 (all)	9 to 12 (all)	15 and 16
4	1 to 4 (all)	5 to 8 (all)	9, 11 and 12	13 to 16 (all)
5	1 to 4 (all)	5 and 7	9, 11 and 12	13 to 16 (all)

Subject 4



Subject 5

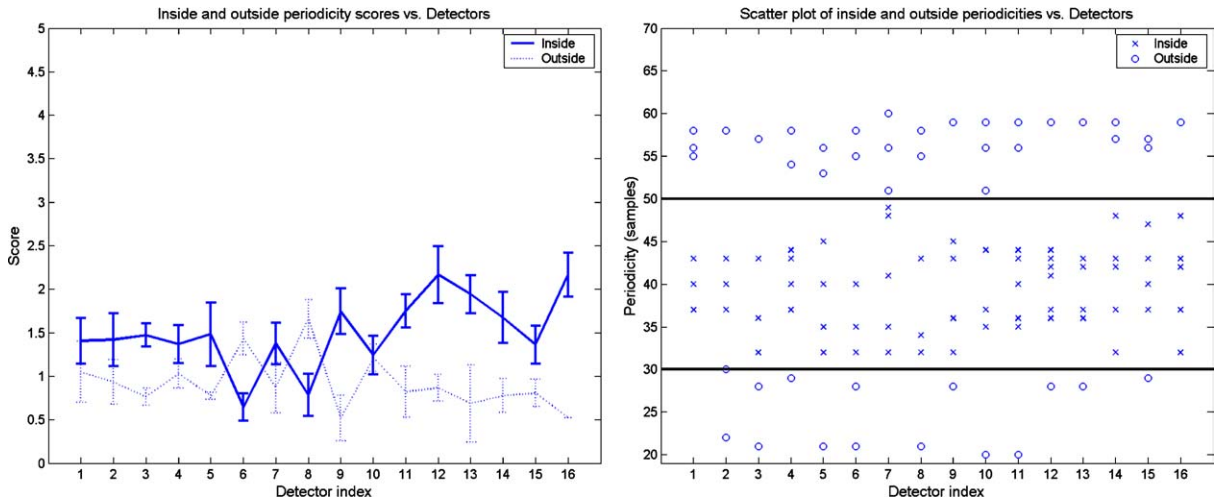


Figure 10. Bar plots of the scores and the scatter plots of the detected periodicities with respect to photodetectors. On the left, the bars indicate standard deviation of data. On the right, thick black bars enclose the expected range of periodicities. In the presented cases, good periodicity is observed in Subject 4 while lesser periodicity exists in Subject 5.

analysis. One popular model is the Gamma function expressed as

$$h(t) = \begin{cases} A(t - T)^2 e^{-(t-T)/\tau} & \text{for } t \geq T \\ 0 & \text{for } t < T \end{cases} \quad (13)$$

where τ is the time-constant that characterizes the response, A is the strength, and T is the delay of the response to the target stimulus. Let's denote the sampled Gamma waveform by the m -dimensional vector \mathbf{h} (where $m = 40$) sampled at the instants

$t = 0, T_s, \dots, (m - 1)T_s, T_s$ being the sampling period (1.7 Hz in the experiment). Implicit in each \mathbf{h} vector is the set of parameters τ and T , where τ is the time-constant that characterizes the response, A is the strength, and T is the delay of the response to the target stimulus. Let's denote the sampled Gamma waveform by the m -dimensional vector \mathbf{h} , constituted of the samples of $h(t)$ in (13) at the instants $t = 0, T_s, \dots, (m - 1)T_s$ and $m = 40$. Consider the fNIRS signal $x(t)$, detrended and, in addition, possibly prefiltered to leave the BC-band, i.e., 30–330 mHz.

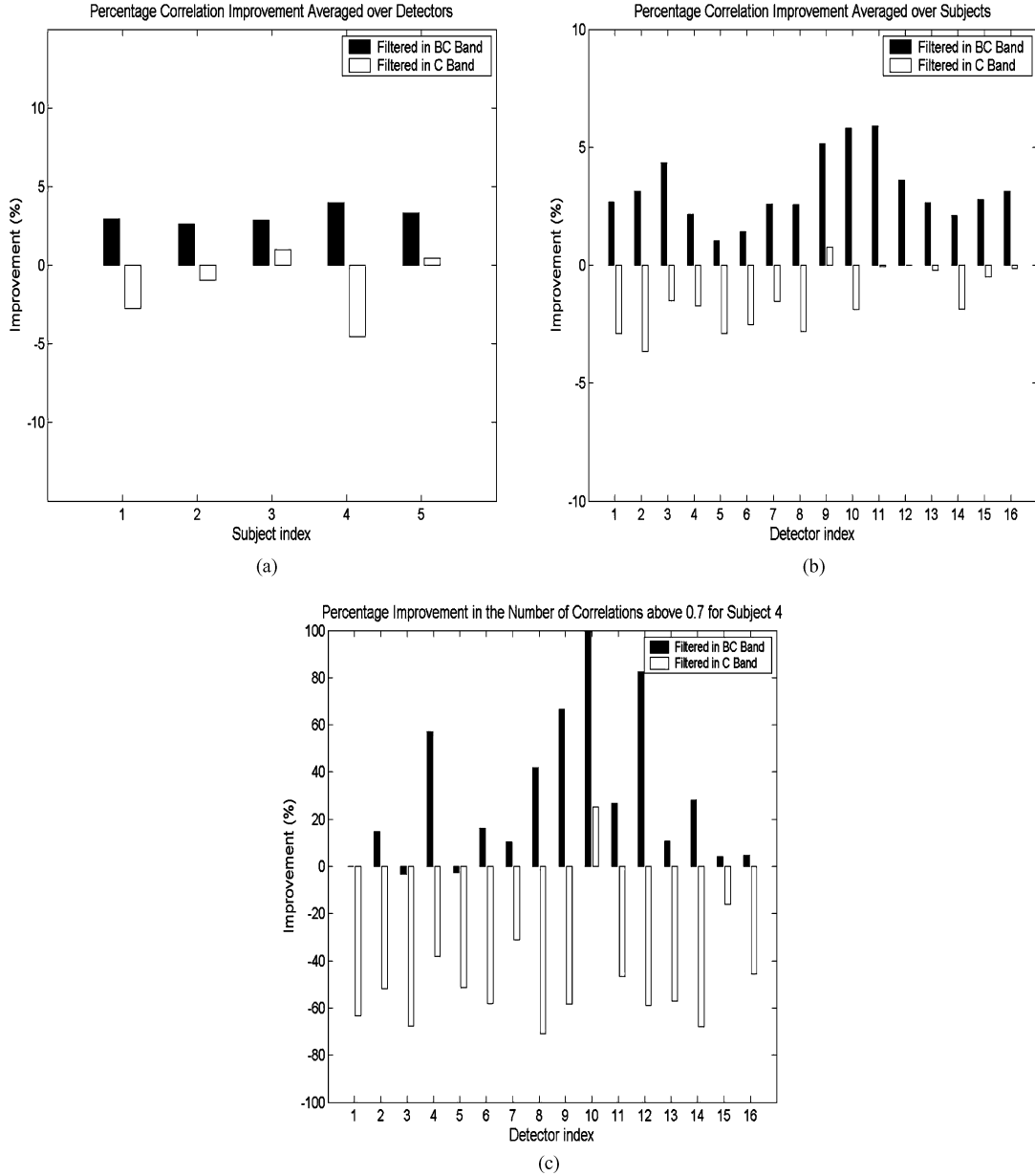


Figure 11. Plots of percentage improvements in the correlation scores with Gamma response model (clockwise): (a) Improvement averaged over all sessions and detectors; (b) Improvements averaged over all sessions and subjects, and (c) Improvement for Subject 4 averaged over all sessions.

- (i) Put into a vector form the 40 samples after each target presentation instant to form one of the \mathbf{z}_k vectors. Recall that there are 64 stimuli per experiment, hence the vector index runs as $k = 1, \dots, 64$.
- (ii) Constrain the time-constant τ of the Gamma waveform in the 1.5–3.5 second range, and the response delay T in the range 0–10 samples. We

search exhaustively for the best match in this parameter space.

- (iii) For each $\mathbf{x}(k)$, find the best match that maximizes the normalized correlation coefficient between $\mathbf{x}(k)$ and \mathbf{h} , i.e.,

$$\rho(k) = \max_{\tau, T} \langle \mathbf{h}, \mathbf{z}_k \rangle$$

where the samples of \mathbf{z}_k that precede the delay T are set to zero.

- (iv) If any prefiltering is used, say we focus on bands B and C , then we denote the correlation as $\rho(k) \equiv \rho_{BC}(k)$, and similarly for other band choices.
- (v) The $\rho(k)$, $k = 1, \dots, 64$ series for all detectors and subjects are pruned out, by deleting low-correlation sessions, such that we keep only those correlations that exceed the threshold of 0.7. Furthermore we calculate the mean of the correlations per detector, $m_\rho(l)$, where the detector index runs over $l = 1, \dots, 16$.

We have computed the mean correlation profiles for the original signals (no prefiltering) and for signals pre-filtered in the BC (30–330 mHz) and C (60–330 mHz) bands. The prefiltering of the AB band (0–60 mHz) was specifically avoided to preclude any resonance effect with the Gamma response model. In Fig. 10, we display some of these mean correlation profiles and bar plots for cases where correlations exceed the threshold of 0.7. As to be expected in the light of the assumed Gamma response, we observe that:

Prefiltering helps in general to improve the correlation scores. In fact, the scores have definitely increased in the BC band, whether considered over subjects or detectors. On the other hand, excluding the B band, that is considering only the C band, we find much lower scores. Another useful note is that the inter-detector variability in the number of encountered Gamma matches decreases in the BC -band. These observations point to the fact that the cognitive activity is mainly localized above 0.03 Hz, that is, in the 30–300 mHz range (Toronov et al., 2000; Prince et al., 2003). The results are illustrated in Fig. 11, where we contrast the percentage change in the number of sessions exceeding the correlation threshold of 0.7 when 30–330 mHz BC -band is considered vis-à-vis the 60–330 C -band or the full ABC -band. One can observe that the correlation scores improve whether observed over subjects or detectors by 10 to 50%.

5. Conclusions

Identification of fNIRS frequency bands where cognitive activity predominates in single-event trials is an important problem. Based on the clustering tendency of time-frequency power spectra, we have determined that there exist three bands of interest: A -band (0–30 mHz), B -band (30–60 mHz) and C -band (60–330 mHz). The

A -band is conjectured to represent the context activity and some cognitive activity. The B -band is predominantly cognitive-activity related, while the C -band accounts for various physiological activities as well as protocol-induced periodicity. Our analysis has covered up to 330 mHz range since this was the cut-off frequency of the built-in RC-filter in the fNIRS device. These bands are found to be very similar to those in related studies (Hu et al., 1999; Kuo et al., 1998; Obrig et al., 2000a; Franceschini et al., 2000; Toronov et al., 2000).

Correlation between the response model waveforms (Gamma waveform) and the fNIRS signals becomes maximum in the joint AB -band (0–60 mHz). On the other hand, protocol-induced periodicity is best observed in the BC -band (60–330 mHz). Since each subject was tested only once, we cannot comment on intra subject variability. We believe that evidence of periodicity in detectors provides a guideline for selecting responsive photodetectors and subjects and discarding non-responsive ones.

Acknowledgments

This work has been sponsored in part by funds from the Defense Advanced Research Projects Agency (DARPA) Augmented Cognition Program and the Office of Naval Research (ONR), under agreement numbers N00014-02-1-0524 and N00014-01-1-0986, and in part by Boğaziçi University Research Fund, BURF 02S101 and Tübitak Project 102E027.

References

- Boas DA, Gaudette T, Strangman G, Cheng X, Marota JJA, Mandeville JB (2001). The accuracy of near infrared spectroscopy and imaging during focal changes in cerebral hemodynamics. *NeuroImage* 13: 76–90.
- Blanco S, Garcia H, Quiroga RQ, Romanelli L, Rosso OA (1995) Stationarity of the EEG Series. *IEEE Engineering in Medicine and Biology Magazine* 14: 395–399.
- Boynton GM, Engel SA, Glover GH, Heeger DJ (1996) Linear systems analysis of functional magnetic resonance imaging in human v1. *J. Neuroscience* 16: 4207–4221.
- Chance B, Anday E, Nioka S, Zhou S, Long H, Worden K, Li C, Turray T, Ovetsky Y, Pidikit D, Thomas R (1998) A novel method for fast imaging of brain function, noninvasively, with light. *Optics Express* 2: 411–423.
- Cordes D, Haughton VM, Arfanakis K, Carew JD, Turski PA, Moritz CH, Quigley MA, Meyerand ME (2001) Frequencies contributing to functional connectivity in the cerebral cortex in resting-state data. *Am. J. Neuroradiol.* 22: 1326–1333.

- Firbank M, Okada E, Delpy DT (1998) A theoretical study of the signal contribution of regions of the adult head to near-infrared spectroscopy studies of visual evoked responses. *Neuro Image* 8: 69–78.
- Franceschini MA, Fantini S, Toronov V, Filiaci ME, Gratton E (2000) Cerebral hemodynamics measured by near-infrared spectroscopy at rest and during motor activation. Proc of the Optical Society of America In Vivo Optical Imaging Workshop Washington. Optical Society of America, DC, pp. 73–80.
- Friedman DH (1977) Pseudo-maximum-likelihood speech pitch extraction. *IEEE Trans. on ASSP* 25: 213–221.
- Giller AC, Hatab MR, Giller AM (1999) Oscillations in cerebral blood flow detected with a transcranial doppler index. *J. Cereb. Blood Flow Metab.* 19: 452–459.
- Hu H, Kuo T, Wong W, Luk Y, Chern C, Hsu L, Sheng W (1999) Transfer function analysis of cerebral hemodynamics in patients with carotid stenosis. *J. Cereb. Blood Flow Metab.* 19: 460–465.
- Kim D, Uğurbil K (2002) Bridging the gap between neuroimaging and neuronal physiology. *Image Anal. Stereol.* 21: 97–105.
- Kuo T, Chern C, Sheng W, Wong W, Hu H (1998) Frequency domain analysis of cerebral blood ow velocity and its correlation with arterial blood pressure. *J. Cereb. Blood Flow Metab.* 18: 311–318.
- Mayhew J, Zheng Y, Hou Y, Vuksanovic B, Berwick J, Askew S, Coffey P (1999) Spectroscopic analysis of changes in remitted illumination: The response to increased neural activity in brain. *Neuroimage* 10: 304–326.
- McCarthy G, Luby M, Gore J, Goldman-Rakic P (1997) Infrequent events transiently activate human prefrontal and parietal cortex as measured by functional MRI. *J. Neurophysiology* 77: 1630–1634.
- Obrig H, Neufang M, Wenzel R, Kohl M, Steinbrink J, Einhaupl K, Villringer A (2000a) Spontaneous low frequency oscillations of cerebral hemodynamics and metabolism in human adults. *Neuroimage* 12: 623–639.
- Obrig H, Wenzel R, Kohl M, Horst S, Wobst P, Steinbrink J, Thomas F, Villringer A (2000b) Near-infrared spectroscopy: Does it function in functional activation studies of the adult brain? *Intr. J. Psychophysiol.* 35: 125–142.
- Prince S, Kolehmainen V, Kaipio JP, Franceschini MA, Boas David, Arridge SR (2003) Time series estimation of biological factors in optical diffusion tomography. *Phys. Med. Biol.* 48: 1491–1504.
- Stoica P, Moses RL (1997) Introduction to spectral analysis. Prentice Hall, NJ, p. 43.
- Strangman G, Culver JP, Thompson JH, Boas DA (2002) A quantitative comparison of simultaneous BOLD fMRI and NIRS recordings during functional brain activation. *Neuroimage* 17: 719–731.
- Strik C, Klose U, Erb M, Strik H, Grodd W (2002) Intracranial oscillations of cerebrospinal fluid and blood flows: Analysis with magnetic resonance imaging. *J. Magn. Res. Imag.* 15: 251–258.
- Svensen M, Kruggel F, von Cramon DY (2000) Probabilistic modeling of single-trial fMRI data. *IEEE Trans. on Med. Imaging* 19: 25–35.
- Toronov V, Franceschini MA, Filiaci ME, Wolf M, Fantini S, Gratton E (2000) Near-infrared study of fluctuations in cerebral hemodynamics during rest and motor stimulation: Spatial mapping and temporal analysis. *Med. Phys.* 27: 801–815.
- Villringer A, Chance B (1997) Non-invasive optical spectroscopy and imaging of human brain function. *Trends in Neuroscience* 20: 4435–4442.
- Wobst P, Wenzel RM, Kohl HO, Villringer A (2001) Linear aspects of changes in deoxygenated hemoglobin concentration and cytochrome oxidase oxidation during brain activation. *Neuroimage.* 13: 520–530.
- Zhang R, Zuckerman JH, Giller CA, Levine BD (1998) Transfer function analysis of dynamic cerebral autoregulation in humans. *Am. J. Physiol. (Heart Circ. Physiol.)* 274: H233–H241.